BIOMECHANICAL MODELLING OF THE BRAIN FOR NEURONAVIGATION IN EPILEPSY SURGERY

K. Miller[1,3], A.C.R. Tavner[1], L.P.M. Menage[1], N. Psanoudakis[1], G. Joldes[1], S.K. Warfield[2], D. Hyde[2], A. Wittek[1]

1
Intelligent Systems for Medicine Laboratory
The University of Western Australia
35 Stirling Highway
Crawley WA 6009, AUSTRALIA
Phone: + (61) 8 6488 8545
Email: karol.miller@uwa.edu.au

2
Computational Radiology Laboratory, Boston Children's Hospital and Harvard Medical School, Boston, Massachusetts, 02115, US.

3
Institute of Mechanics and Advanced Materials, Cardiff School of Engineering
Cardiff University, Wales, UK

1 Introduction

It is commonly believed that epilepsy can be treated and managed, but ultimately not cured; a quick internet search for ‘epilepsy’ will confirm this. However this is not the case, as amongst the more medically informed it is well known that precisely-targeted surgery is a curative treatment (Engel 2003). Engel also argues that the surgical treatment of epilepsy is “arguably the most underutilised of all proven effective therapeutic interventions in the field of medicine” (Engel 2003). The explanation for this apparent under-use of surgery to cure epilepsy lies in the phrase “precisely-targeted”: clinicians are often unable to characterise or locate epileptic activity within the brain accurately enough to identify which regions to resect and proceed with surgery (Noachtar and Borggraefe 2009).

In this Chapter we describe how computational biomechanics of the brain (see also Chapter 6 in this book) can help to precisely and reliably locate seizure onset zones (SOZ) and visualise them with respect to pre-operative brain anatomy as part of a system to improve intra-operative visualisation, navigation and monitoring.

1.1 Background

Epilepsy is a chronic neurological disorder that affects over 70 million people, costs over $50 billion annually, and first arises during childhood for 75% of patients (NINDS 2007). Surgical intervention can be curative but is rarely used because of difficulties with localisation of epileptogenic regions of the brain and subsequent surgical planning. When MRI-visible lesions are not present, surgical planning must rely on functional localization. Intracranial EEG (iEEG) is the most effective method for functional localisation of the SOZ; invasive electrodes are implanted and monitored for several days, and then removed during a second

surgery when the resection is performed (Bauman, Feoli et al. 2008). Collecting data from directly on or within the cortex significantly increases the spatial data fidelity when compared to scalp EEG measurements and allows more accurate identification and location of the SOZ.

Despite being the most accurate available technology for monitoring seizure activity, iEEG does not guarantee surgical success. Unsuccessful surgeries are performed, in part, due to difficulties in the clinical interpretation of the measured invasive data. In current practice, electrodes are aligned to the cortex using a combination of intra-operative photographs and diagrams to estimate the placements of electrode grids and depth electrodes. While this allows generalised alignment, it is not quantitative and does not provide the degree of accuracy necessary for emerging precision surgical techniques such as radio frequency (RF) and laser ablation (Curry, Gowda et al. 2012, Tovar-Spinoza, Carter et al. 2013), and focused ultrasound (Monteith, Sheehan et al. 2013). To fully utilise the precision of these emerging techniques, accurate alignment algorithms are needed to enable precise identification of the SOZ with respect to both pre-operative and intra-operative imaging.

A significant factor contributing to electrode alignment error is the physical shifting of brain tissue during invasive measurement (see Figure 1). Electrode grids in the intracranial space, and the body's inflammatory response to the craniotomy, displace and deform the brain from the configuration observed in pre-surgical MR imaging (Wittek, Joldes et al. 2010, Taimouri, Akhondi-Asl et al. 2014). To ensure accurate alignment of electrode placements and correct clinical evaluation of invasive data, brain shift must be accurately modelled and accounted for.

In Chapter 6 we described in detail effective approaches for computing brain deformations during neurosurgery. In this Chapter we focus on applying these modelling methods to the particularly challenging and clinically relevant problem of the registration of pre-operative MRI to intra-operative CT (with electrodes implanted) images.

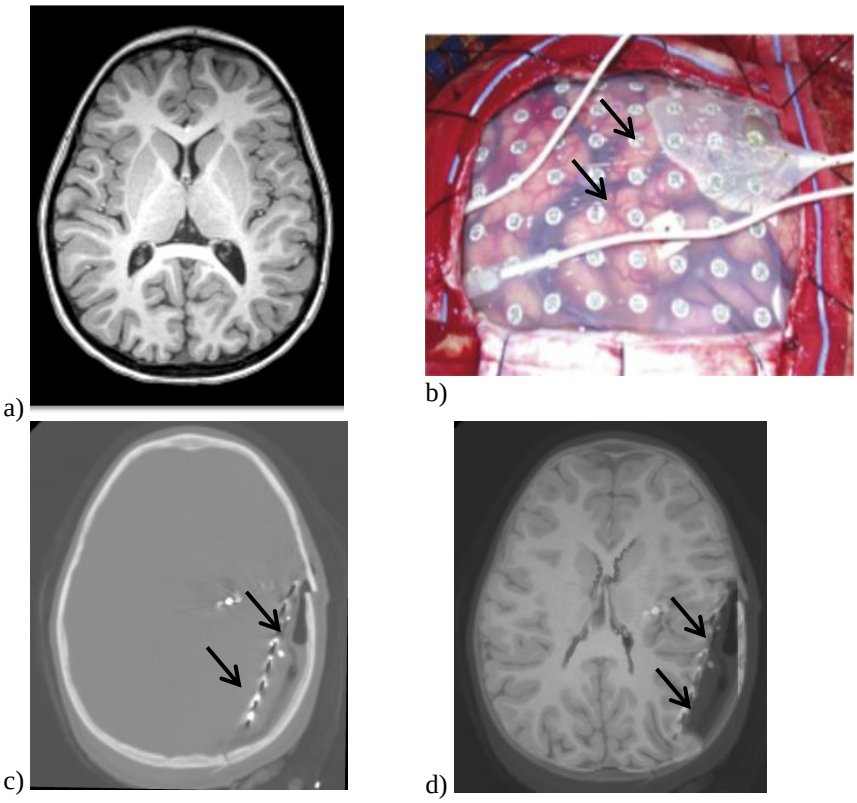

Figure 1: a) Pre-operative MRI, b) intra-operative photograph of implanted intracranial electrodes (pointed by arrows), c) intra-operative CT with electrodes implanted, and d) pre-operative MRI registered onto intra-operative CT. In this Chapter we explain how to obtain image 1d using computational biomechanics of the brain. These are 2-dimensional sections of 3-dimensional image volumes. We have successfully registered four cases (Menagé 2017).

Accurate registration is achieved using reliable computation of the deformations within the brain due to invasive electrode placement. An accurate model of brain shift enables us to accurately map pre-surgical imaging onto the deformed intra-operative space, accurately aligning these scans with X-Ray CT (Figure 1), thereby providing the location of electrodes as well as the SOZ identified by them relative to the anatomical structures of the brain as seen on pre-operative MRI 'warped' onto intra-operative CT images.

1.2 Modelling the Intra-Operative Deformation

A recent review (Gerard, Kersten-Oertel et al. 2017) summarises brain shift causes, measurements and compensation methods. Modelling the behaviour of the brain remains a key issue to provide *a priori* knowledge for image-guided surgery. The biomechanical

property experiments of Miller (Miller 2011) and others (see e.g. (Bilston 2011)) significantly contributed to the understanding of the physics of brain tissue. We also quantified the relative importance of various parameters required for accurate modelling of intra-operative deformations of the brain, such as geometry, boundary conditions, loading and constitutive properties, see Chapter 6 of this book and (Miller 2011). Moreover, we have developed very computationally-efficient algorithms that allow the equations describing brain biomechanical models to be solved intra-operatively (i.e. in less than 10 sec) on standard computing hardware (Joldes, Wittek et al. 2010).

A number of groups have investigated the use of intra-operative ultrasound in order to provide data that could be used to update pre-operative models to account for brain shift (Reinertsen, Lindseth et al. 2014, Rivaz and Collins 2015). Laser range scanners (LRS) (Sun, Lunn et al. 2005, Miga, Sun et al. 2016) and stereo cameras (Sun, Lunn et al. 2005) have also been used. However the data obtained using these techniques cannot be directly used for surgical navigation, as images typically have poor contrast and resolution, and surface data alone is not sufficient to guide neuronavigation.

Summary

1. Inaccuracies in the identification of invasive electrode placements and the limited ability to relate the SOZ identified by these electrodes to features of brain anatomy prevent iEEG data from being fully utilised to identify appropriate resection regions.
2. A method to reliably and precisely identify the location of seizure onset zones could lead to curing millions of patients of epilepsy.
3. The key technology we describe in this Chapter is biomechanics-based prediction of brain deformations resulting from the invasive electrode placement, and the use of these

deformations to register a pre-operative MRI image onto an intra-operative CT image with electrodes in place (Figure 1d).

In Section 2 we describe how to adapt the methods presented in Chapter 6 to model brain deformations resulting from invasive electrode placement. In Section 3, to demonstrate the appropriateness and effectiveness of our biomechanics-based methods, we consider results of brain deformation computation for a specific example of a paediatric epilepsy patient from Boston Children's Hospital. The numerical algorithms devised to efficiently solve brain deformation models are described in Chapters 10 and 11.

2. Computing brain deformations due to insertion of invasive electrodes

Biomechanical modelling issues related to **geometry and finite element mesh, boundary conditions, loading and material properties** are briefly summarised below. For a more detailed discussion of these issues please refer to Chapter 6.

A high-level depiction of the inputs, outputs and software packages used in each step of the analysis is shown in Figure 2 below.

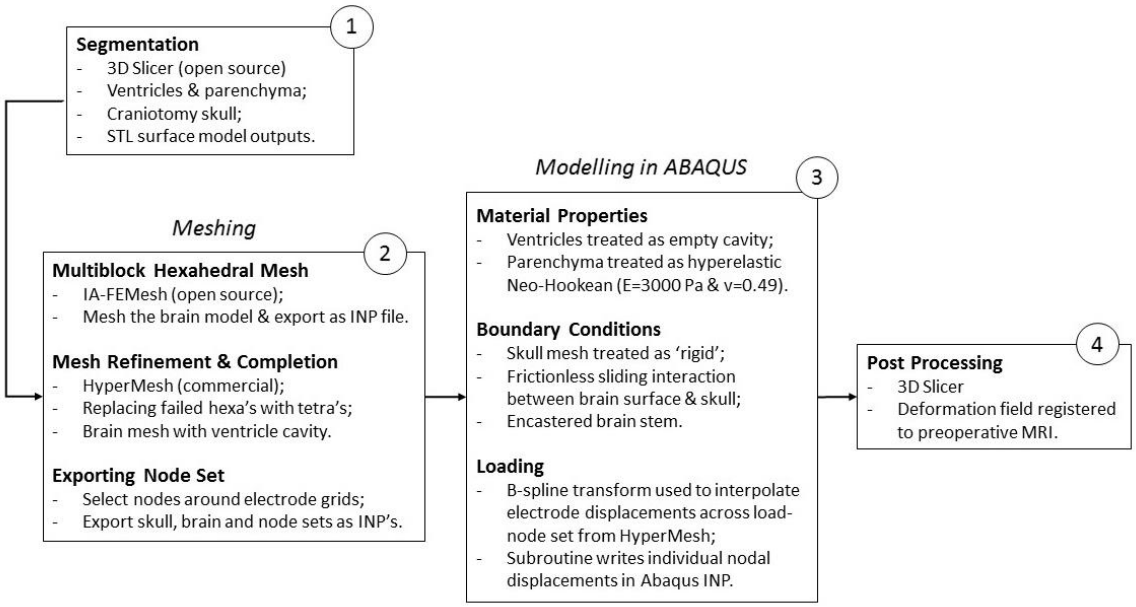

Figure 2: Model Formulation Diagram

2.1 Geometry

The first step in the construction of model geometry is to develop surface models of the brain parenchyma and ventricles. 3D Slicer (http://www.slicer.org/) is used to segment the regions of interest (ROI) from the patient's MRI with the help of automated thresholding tools. The

data is segmented into three separate label maps, including the CSF in red, white matter in green and grey matter in blue (Figure 3).

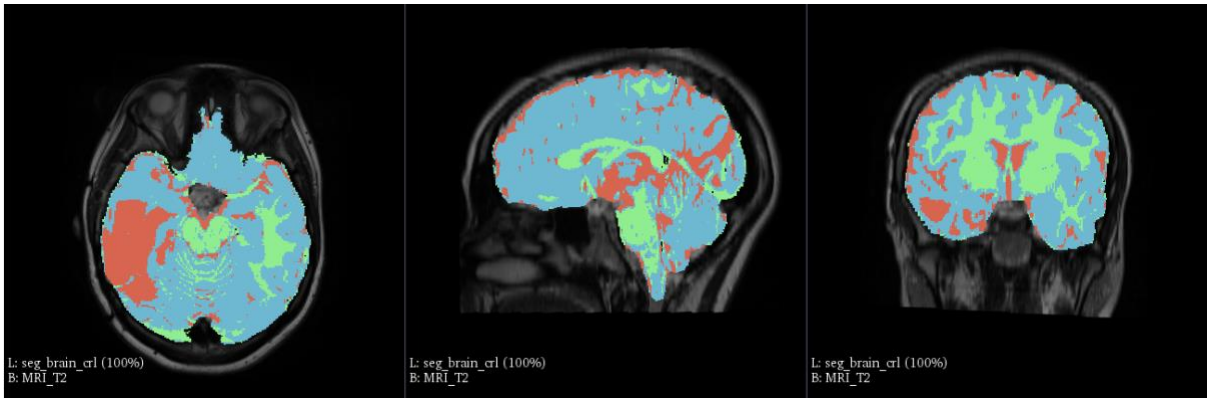

Figure 3: Boston Children's Hospital Segmentation Maps; Anonymous Case 192

This map is then manually edited to remove the cerebellum, which simplifies the mesh generation and computational analysis. The cerebellum is not mechanically integral with the left and right hemispheres and can therefore be ignored from the analysis. Label map smoothing is also needed to remove the detail of deep sulci and fissures, which are problematic for mesh generation. If the smoothing process is carefully controlled, there is little impact on the deformation computed within the ROI of the brain. The *LabelStatistics* module is used to check the voxel count before and after smoothing to ensure that the smoothing never results in more than 3% volume change. Visual inspection of the sagittal, axial and coronal views also helps to maintain accuracy in the segmentation. Finally, the smoothed label map is exported as an STL surface model, ready for meshing.

The contrast and resolution of the MRI data in the area surrounding the ventricles makes it difficult to accurately apply thresholding and marching algorithms, so the ventricle segmentation must be performed almost entirely by hand. The label map is again smoothed, to

remove surface imperfections, and exported as an STL file. The completed surface models are shown in Figure 4 below.

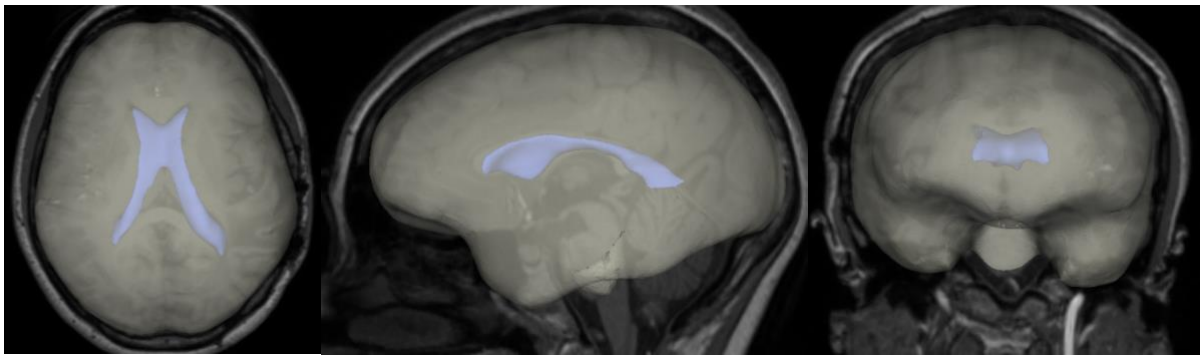

Figure 4: Segmented parenchyma and ventricles surface models

2.2 Finite element meshing

To create the hexa-dominant mesh required for reliable computations (see Chapters 5 and 10) of a geometry as irregular as the brain, a multiblock method is applied through the open source package IA-FEMesh from the University of Iowa (https://www.ccad.uiowa.edu/MIMX/projects/IA-FEMesh). The parenchyma surface model is loaded into the program and a centralised block is created around it. The block is then split into smaller interconnected grids whose nodes can be dragged to fit closer around the surface of the model (Figure 5a). A completely hexahedral mesh is generated by seeding the edges and projecting through each of the blocks (Figure 5b).

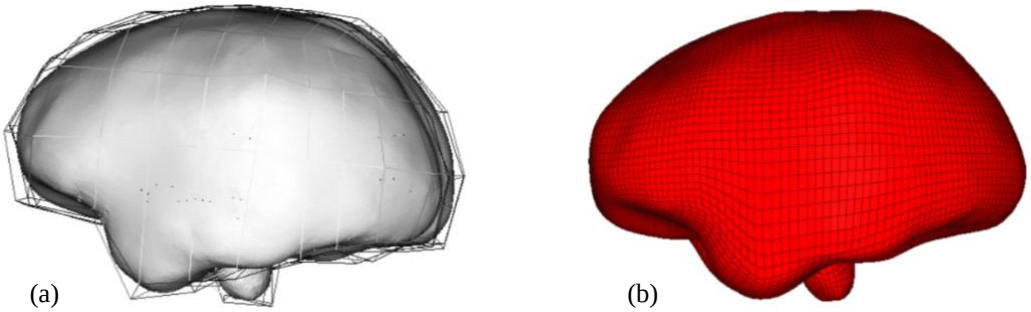

(a) (b)

Figure 5: Multiblock meshing in IA-FEMesh: (a) Blocks; (b) Mesh

The resulting mesh features good quality hexahedral elements throughout most of the volume, but poor-quality elements close to the surface and around complex changes in geometry. To identify and improve these elements, the model is loaded as an input (INP) file into HyperMesh (https://altairhyperworks.com/product/hypermesh) and quality checks are performed for the warpage, element length and Jacobian characteristics. As discussed in Chapters 5 and 10, the metrics to apply in biomechanical models are uncertain and depend on the situation. In this case, it was found that the following targets give a mesh of sufficient quality:

- Warpage: 90°
- Length: 0.5 mm
- Jacobian: 0.5

Elements that fail to meet these criteria are isolated into a separate component and converted into tetrahedral elements before being merged back into the original mesh. Next, the ventricles are imported and a 2D triangular mesh is generated across the surface. To integrate the two components into a single mesh, elements surrounding the ventricles in the parenchyma model are removed to create a void between the two. By selecting the internal faces of this void, tetrahedral elements can be propagated from the brain elements to the 2D surface elements on the ventricles, as shown in Figure 6.

The final steps in HyperMesh are to create a surface mesh for the skull, which is necessary for modelling the brain/skull interface. The skull is created by copying the outer faces of the brain mesh, offsetting the elements outward by 0.1 mm to prevent overlap, and creating openings at the brain stem and craniotomy. The shape and location of the craniotomy opening in the skull is best obtained by segmenting the skull from the patient's intra-operative CT scan and loading the geometry into HyperMesh as a new component (Figure 7).

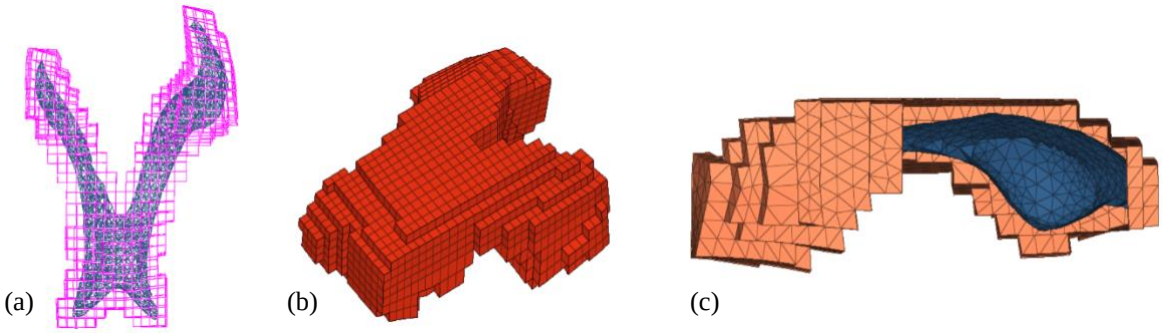

Figure 1: (a) Boolean elements; (b) Faces surrounding void; (c) Filled tetrahedral elements

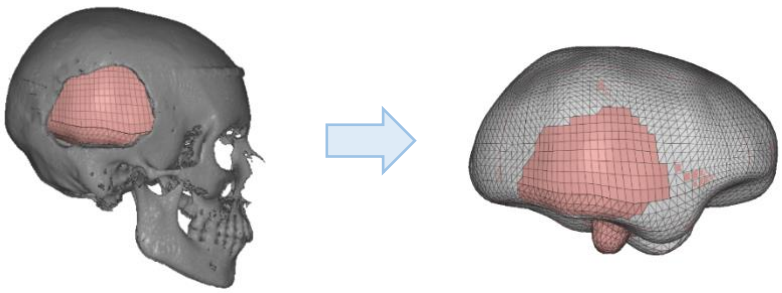

Figure 7: Skull mesh

Before exporting the brain and skull meshes, a node set must be created for applying the measured surface displacement loading (see Section 2.4 of this Chapter). To do this, the patient's 3D coordinate data for the electrodes in their pre-operative position are converted to

an STL surface model and loaded into HyperMesh. As shown in Figure 8 below, this allows the elements encompassing the electrodes to be isolated, and then by previewing the nodal equivalence between the selected elements and the original brain mesh, it is possible to save a nodal set corresponding to the displaced surface.

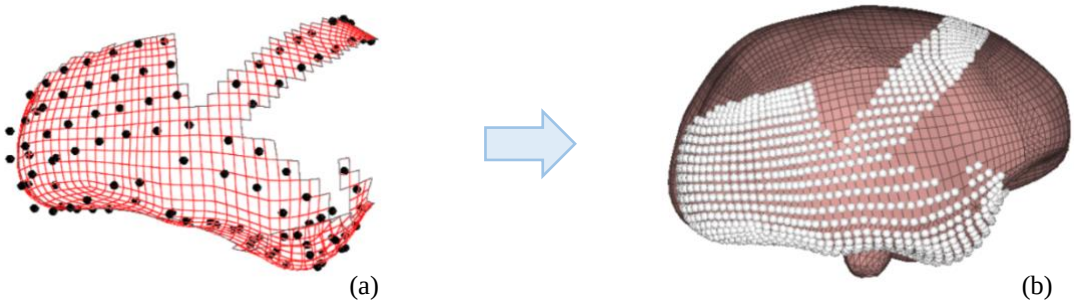

(a) (b)

Figure 8: (a) Preoperative electrodes on brain mesh; (b) Selected node set

Finally, the meshed parts and node set are exported and combined into a single INP file for importing into Abaqus for analysis. Table 1 summarises the mesh attributes.

Table 1: Mesh Characteristics

	Brain	***Skull***
No. Elements (Nodes)	48,953 (24,213)	8,056 (4,073)
Element type(s)	4-noded Tetrahedral (66.3% elements) 8-noded Hexahedral (33.7% elements)	3-noded triangles
Node set	950 nodes	N/A

2.3 Boundary conditions

As explained in Chapter 6, frictionless sliding contact between the brain and the skull is an appropriate choice for the model's boundary condition. We implement this in Abaqus by defining a general surface interaction with a *hard* contact behaviour and a *frictionless* interaction property (equivalent to a penalty condition of 0). Abaqus applies this interaction by calculating the relative overclosure (penetration) of a deforming body into the rigid surface, and subsequently modelling the kinematic contact and shear sliding (ABAQUS

2013). The remaining boundary conditions in the initial step include assigning a *rigid-body* constraint to the skull, fixing a reference point on the skull mesh in space, and fixing a selection of nodes along the base of the brainstem.

2.4 Loading

We load the model through imposed displacements on the model surface, see Chapter 6 and (Wittek, Joldes et al. 2010). In intra-operative CT (Fig. 1c) the implanted electrodes, and the grid which define the deformed surface of the brain, are clearly visible. Rigid alignment of pre-operative MRI with intra-operative CT and projection of the electrode positions onto the deformed brain surface (seen on CT) from the un-deformed brain surface (seen on the pre-operative MRI) allows precise definition of surface displacements (Taimouri, Akhondi-Asl et al. 2014).

Using the intra-operative and pre-operative electrode coordinates, we define a B-spline transform using the *Scattered Transform*[1] module in 3D Slicer. The B-spline transform interpolates the difference between the intra-operative and pre-operative electrode coordinates across all points within the node set defined in HyperMesh. This allows us to calculate an approximation of the intra-operative position of the surface nodes in the brain mesh. To apply the transform, the INP file containing the node set coordinates is first converted into a VTK format so that it can be read into 3D Slicer. Once transformed, the data is converted back to a text-based or csv format so that it can be read into MATLAB for processing. Figure 9 below is a visual representation of the electrode transform applied to the node set from HyperMesh. The MATLAB script was written to import the two data sets, compute the displacements and subsequently write each displacement as an Abaqus-compatible nodal boundary condition in

INP format. In this case, the subroutine outputs 2850 individual boundary conditions, which are easily transferred to the INP file containing the part and element definitions, before loading into Abaqus CAE for analysis.

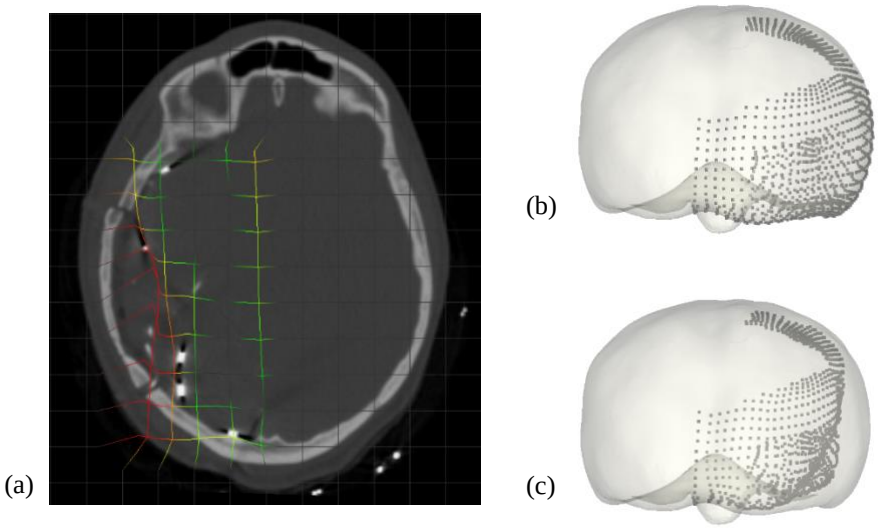

Figure 9: (a) Electrode transform in 3D Slicer; (b) Preoperative node set; (c) Node set transformed to the intraoperative position

The loading is applied gradually over a period of 10 seconds using the *Smooth Step* amplitude function in Abaqus, which implements a 345 polynomial (ABAQUS 2013). This is necessary to prevent excessive distortion in the elements resulting from large displacement increments in each time step.

2.5 Material properties

As explained in Chapter 6 of this book and our papers (Wittek, Hawkins et al. 2009, Miller and Lu 2013)**,** for problems where loading is prescribed as forced motion of boundaries, the unknown deformation field within the domain only depends very weakly on the mechanical properties of the continuum. This feature is of great importance in biomechanical modelling where there are always uncertainties in patient-specific properties of tissues. Therefore we use

[1] https://www.slicer.org/wiki/Documentation/Nightly/Extensions/ScatteredTransform

a simple Neo-Hookean (Wittek, Hawkins et al. 2009) constitutive model with Young's Modulus of 3000 Pa. To account for approximate incompressibility of brain tissue (see Chapter 4 of this book) we chose a Poisson's ratio of 0.49.

2.6 Solution algorithm and software

Although the analysis is static, an explicit algorithm is the preferred solver because the non-linearity of the model makes it difficult and computationally expensive to achieve convergence in every time step (see Chapter 10). The model is run in ABAQUS Explicit for 100 simulation seconds to allow sufficient time for a steady state solution to be achieved. To ensure stability, a minimum time step has been estimated from the characteristic length of the mesh and the dilatational wave speed (ABAQUS 2013) to be ca. 4×10^{-5} seconds. The default parameters for linear and quadratic bulk viscosity are used, providing a means of damping to control high-frequency oscillations in the solution.

The element formulations available in Abaqus Explicit include linear or quadratic elements. For efficiency, the linear reduced integration hexahedrons (C3D8R) and tetrahedrons (C3D4) are chosen with default hourglass and distortion control (for discussion about appropriate element types for explicit analysis of approximately incompressible materials see also Chapters 6 and 10 of this book). The skull is assigned rigid triangular facet elements (R3D3).

3 Results

Figure 10 shows the computed deformation along the loaded surface of the brain, whilst Figure 111 shows a comparison of internal sectional views, before and after the simulation.

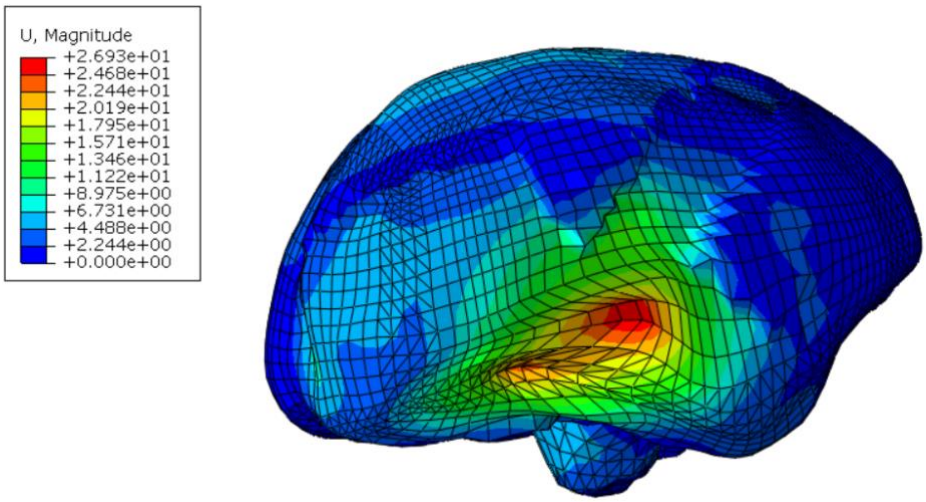

Figure 2: Isometric view of deformed brain

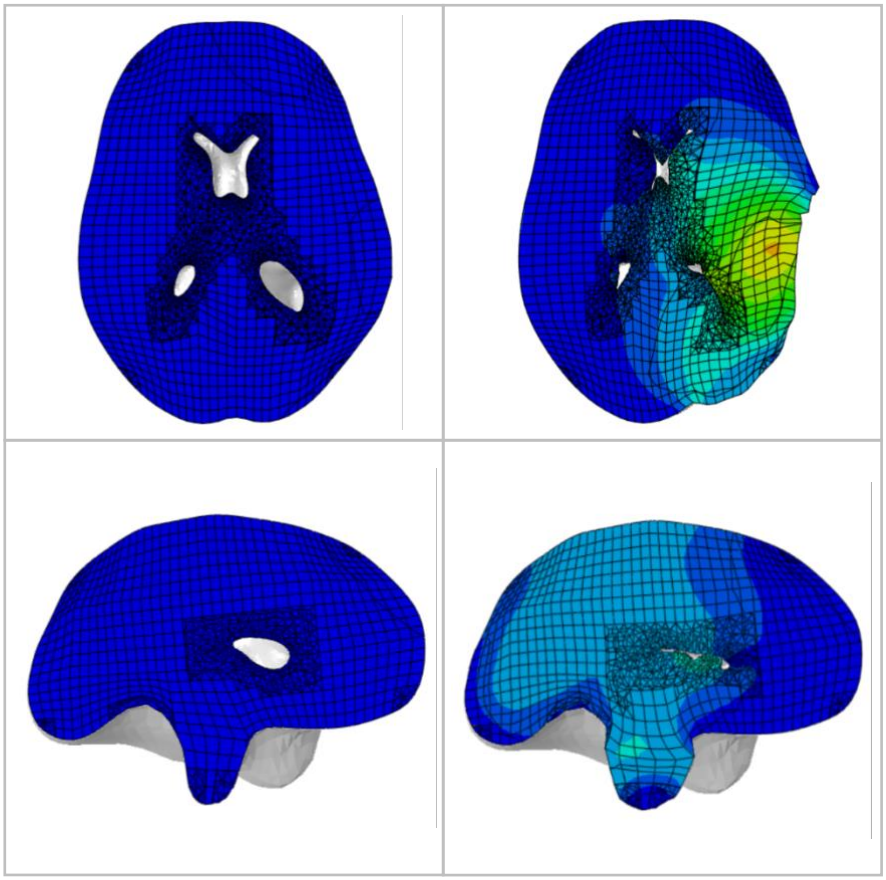

Figure 11: Sectional views of deformed brain

It should be noted that some areas of the model are being displaced by up to 20 mm. Figure 11 also shows a significant amount of compression in the ventricles, which reflects the modelling assumption that enough time passes for the CSF to be displaced. The visualisation of these results illustrates the complexity of the internal brain shift and the severity of the inaccuracies that exist in current localisation practices. It is also important to note that volumetric locking is commonly an issue for first order tetrahedral elements in an almost incompressible media. Although the tetrahedral elements around the ventricles show quite large deformations on the load-side, the results could be an under-representation of reality if artificial stiffening is present – particularly on the opposite side of the brain (left hemisphere).

The images above also show a rather blocky and unnatural edge along the indentation where the electrode displacements have been applied. We believe that this unnatural curvature in the deformed model is a result of the mesh quality. The elements within these problematic areas can be up to 11 mm, even though the average element is approximately 4 mm for the rest of the model. This means that the elements are probably too large to capture the smoothness of the deformation in these regions of extreme compression.

In assessing the reliability of the results, we note that a comparison of the energy and displacement outputs over time suggests that a bounded solution has been achieved. Figure 12 shows a plot of various energy variables computed over time; including internal energy

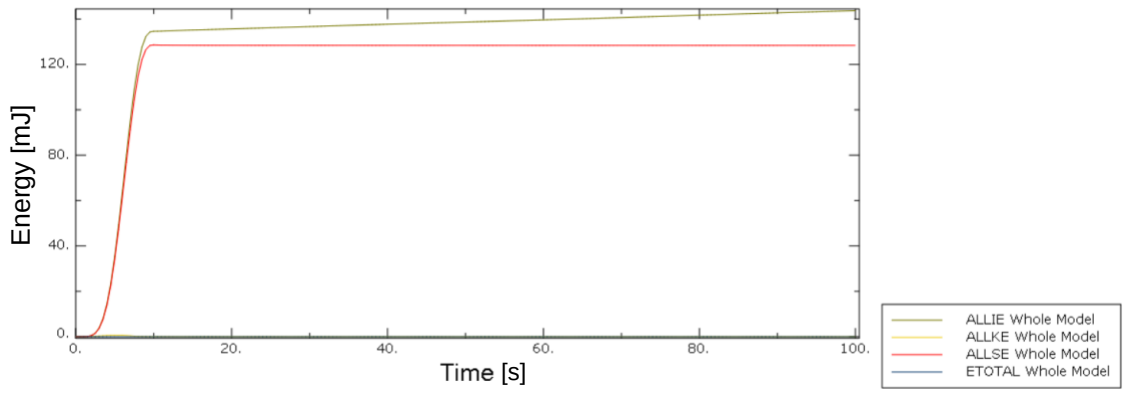

Figure 3: Plot of energy over time

(ALLIE), kinetic energy (ALLKE), total energy (ETOTAL) and strain energy (ALLSE), which all appear to show stability in the solution output. The displacement of a node along the loaded-side of the ventricle cavity is shown in Figure 13, which also shows a steady state result after about 60 simulation seconds.

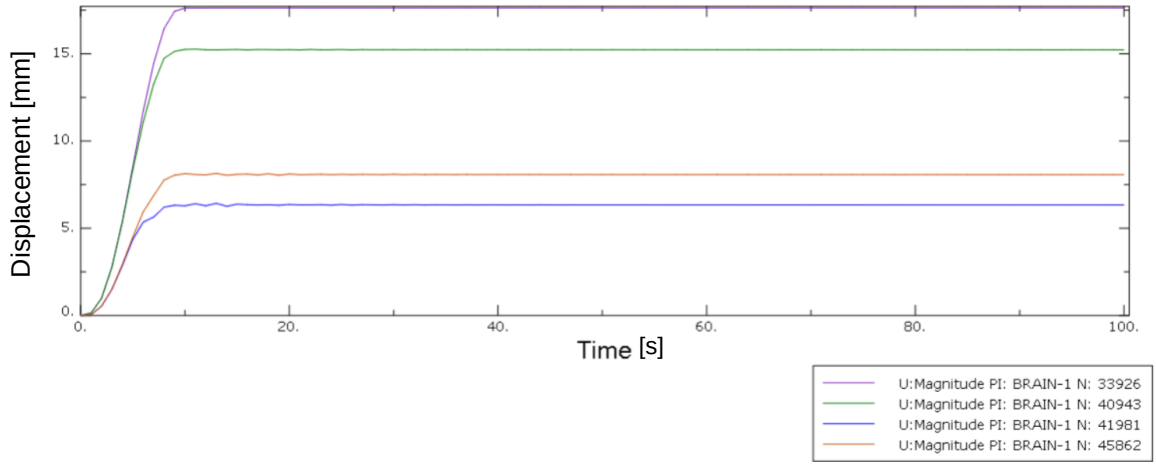

Figure 4: Nodal displacement at ventricle wall over time

The computed nodal displacements are then used to warp pre-operative MRI. Warping the MRI is achieved by exporting the deformed nodal coordinates and using them to create another B-spline transform in the 3D Slicer *Scattered Transform* module (Joldes 2017). The transform is then applied to interpolate the computed deformation field across all voxels in the MRI and warp the image to the intraoperative position.

The result of the transform applied to the MRI is shown in Figure 14b. The transform closely reflects the deformation field shown in the Abaqus results, and overlaying the transformed MRI with the intraoperative CT (Figure 14c) shows that the electrodes are visibly aligned with the edge of the MRI. This result achieves the overall objective of this Chapter, by demonstrating that a biomechanical model *can* be used to solve for the internal deformation field of a patient-specific epilepsy case and warp the pre-operative MRI to the intra-operative position. Comparing the poor resolution and detail of the CT in Figure 14a, to the overlaid

image in Figure 14c, it is clear to see the vast improvement in accuracy that is possible with patient-specific modelling.

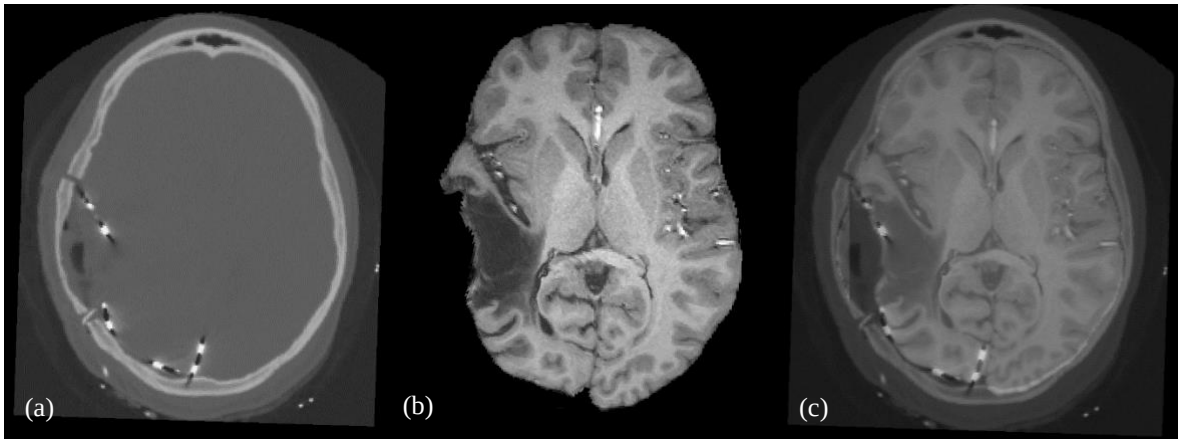

Figure 5: (a) Intraoperative CT; (b) Transformed MRI; (c) Transformed MRI overlaid on CT

4. Conclusions

The surgical treatment of epilepsy has the potential to permanently cure seizures, but the process is hindered by the inability to confidently locate the seizure onset zone (SOZ) in the planning stage. Through the analysis of a real, patient-specific case from the Boston Children's Hospital, we have shown that it is possible to apply biomechanical modelling and Finite Element Methods to compute the deformation field within the brain arising from invasive electrode placement, and warp a pre-operative MRI into the intra-operative configuration of the brain. This provides a highly detailed map of the electrodes relative to neurological landmarks, making it easier to confidently identify what tissue to resect and how. The generation of the finite element mesh and model input took an experienced analyst approximately two days. This is acceptable in the research environment but too long for compatibility with existing clinical workflows. Further work into more efficient methods of patient-specific model generation is clearly needed (see Chapters 10 and 11 of this book).

The model was analysed in Abaqus for 100 simulation seconds, which took approximately 2 hours to complete and a further hour to process the results and register the deformation field. As close-to-real-time processing speeds are not demanded by this application, these simulation and analysis times are compatible with existing clinical workflows and further improvements, while helpful, are not strictly necessary. These timeframes would fit within the 5-7-day period of data collection while the electrodes are on the brain.

The accuracy of segmentation is a limitation that affects the accuracy of the model geometry. Segmentation remains a challenging and subjective process that does not guarantee repeatability. Improvements in this area can only really come from research into improved imaging and more robust segmentation algorithms, however it is likely that manual input will always be required in this process. For example, intensity and label fusion algorithms have

demonstrated very high reproducibility and accuracy indistinguishable from that of human experts (Akhondi-Asl and Warfield 2013, Akhondi-Asl, Hoyte et al. 2014, Velasco-Annis, Akhondi-Asl et al. 2018).

Because manual surgery cannot achieve accuracy better than 1 mm, even slight deviations by one or two voxels can still produce a better method of localisation than is currently used in practice.

Finally, another area of interest in the surgical treatment of epilepsy is in the modelling of depth electrodes. These are very long and slender needles that pierce deep into the parenchyma and are extremely difficult to control and locate during their insertion. Surgeons may benefit from the ability to predict how the needle will behave in the tissue, or be able to practice using haptic feedback simulations before they conduct the operation on the patient.

Acknowledgements

The funding from the Australian Government through the Australian Research Council ARC (Discovery Project Grants DP160100714, DP1092893, and DP120100402) and National Health and Medical Research Council NHMRC (Project Grants APP1006031 and APP1144519) is greatly acknowledged. We thank the Raine Medical Research Foundation for supporting G. R. Joldes through a Raine Priming Grant, and the Department of Health, Western Australia, for funding G. R. Joldes through a Merit Award. This investigation was also supported in part by NIH grants R01 NS079788, R01 EB019483, R42 MH086984 and by a research grant from the Boston Children's Hospital Translational Research Program.

References

ABAQUS (2013). ABAQUS Theory Manual Version 6.13. Providence, RI, Dassault Systèmes Simulia Corp.

Akhondi-Asl, A., L. Hoyte, M. E. Lockhart and S. K. Warfield (2014). "A logarithmic opinion pool based STAPLE algorithm for the fusion of segmentations with associated reliability weights." IEEE Trans Med Imaging **33**(10): 1997-2009.

Akhondi-Asl, A. and S. K. Warfield (2013). "Simultaneous truth and performance level estimation through fusion of probabilistic segmentations." IEEE Trans Med Imaging **32**(10): 1840-1852.
Bauman, J. A., E. Feoli, P. Romanelli, W. K. Doyle, O. Devinsky and H. L. Weiner (2008). "Multistage epilepsy surgery: safety, efficacy, and utility of a novel approach in pediatric extratemporal epilepsy." Neurosurgery **62 Suppl 2**: 489-505.
Bilston, L. E., Ed. (2011). Neural Tissue Biomechanics. Studies in Mechanobiology, Tissue Engineering and Biomaterials, Springer.
Curry, D. J., A. Gowda, R. J. McNichols and A. A. Wilfong (2012). "MR-guided stereotactic laser ablation of epileptogenic foci in children." Epilepsy & behavior : E&B **24**(4): 408-414.
Engel, J., Jr. (2003). "A Greater Role for Surgical Treatment of Epilepsy: Why and When?" Epilepsy Curr **3**(2): 37-40.
Gerard, I. J., M. Kersten-Oertel, K. Petrecca, D. Sirhan, J. A. Hall and D. L. Collins (2017). "Brain shift in neuronavigation of brain tumors: A review." Medical Image Analysis **35**: 403-420.
Joldes, G. R. (2017). "Scattered Transform - a 3D Slicer extension.", from https://github.com/grandwork2/ScatteredTransform.
Joldes, G. R., A. Wittek and K. Miller (2010). "Real-time nonlinear finite element computations on GPU - application to neurosurgical simulation." Computer Methods in Applied Mechanics and Engineering(199): 3305-3314.
Menagé, L. P. M. (2017). Computer Simulation of Brain Deformations for the Surgical Treatment of Paediatric Epilepsy. Master of Engineering, The University of Western Australia.
Miga, M. I., K. Sun, I. Chen, L. W. Clements, T. S. Pheiffer, A. L. Simpson and R. C. Thompson (2016). "Clinical evaluation of a model-updated image-guidance approach to brain shift compensation: experience in 16 cases." International Journal of Computer Assisted Radiology and Surgery **11**(8): 1467-1474.
Miller, K., Ed. (2011). Biomechanics of the Brain. New York, Springer.
Miller, K. and J. Lu (2013). "On the prospect of patient-specific biomechanics without patient-specific properties of tissues." Journal of Mechanical Behavior of Biomedical Materials **27**: 154–166.
Monteith, S., J. Sheehan, R. Medel, M. Wintermark, M. Eames, J. Snell, N. F. Kassell and W. J. Elias (2013). "Potential intracranial applications of magnetic resonance-guided focused ultrasound surgery." Journal of neurosurgery **118**(2): 215-221.
NINDS (2007). Curing The Epilepsies: The Promise of Research, NINDS.
Noachtar, S. and I. Borggraefe (2009). "Epilepsy surgery: a critical review." Epilepsy & behavior : E&B **15**(1): 66-72.
Reinertsen, I., F. Lindseth, C. Askeland, D. H. Iversen and G. Unsgård (2014). "Intra-operative correction of brain-shift." Acta Neurochirurgica **156**(7): 1301-1310.
Rivaz, H. and D. L. Collins (2015). "Deformable registration of preoperative MR, pre-resection ultrasound, and post-resection ultrasound images of neurosurgery." International Journal of Computer Assisted Radiology and Surgery **10**(7): 1017-1028.
Sun, H., K. E. Lunn, H. Farid, W. Ziji, D. W. Roberts, A. Hartov and K. D. Paulsen (2005). "Stereopsis-guided brain shift compensation." IEEE transactions on medical imaging **24**(8): 1039-1052.
Taimouri, V., A. Akhondi-Asl, X. Tomas-Fernandez, J. M. Peters, S. P. Prabhu, A. Poduri, M. Takeoka, T. Loddenkemper, A. M. Bergin, C. Harini, J. R. Madsen and S. K. Warfield (2014). "Electrode localization for planning surgical resection of the epileptogenic zone in pediatric epilepsy." Int J Comput Assist Radiol Surg **9**(1): 91-105.

Tovar-Spinoza, Z., D. Carter, D. Ferrone, Y. Eksioglu and S. Huckins (2013). "The use of MRI-guided laser-induced thermal ablation for epilepsy." Child's nervous system : ChNS : official journal of the International Society for Pediatric Neurosurgery **29**(11): 2089-2094.
Velasco-Annis, C., A. Akhondi-Asl, A. Stamm and S. K. Warfield (2018). "Reproducibility of Brain MRI Segmentation Algorithms: Empirical Comparison of Local MAP PSTAPLE, FreeSurfer, and FSL-FIRST." J Neuroimaging **28**(2): 162-172.
Wittek, A., T. Hawkins and K. Miller (2009). "On the unimportance of constitutive models in computing brain deformation for image-guided surgery." Biomechanics and modeling in mechanobiology **8**: 77-84.
Wittek, A., G. Joldes, M. Couton, S. K. Warfield and K. Miller (2010). "Patient-specific non-linear finite element modelling for predicting soft organ deformation in real-time; Application to non-rigid neuroimage registration." Progress in Biophysics and Molecular Biology **103**: 292-303.
Wittek, A., G. R. Joldes, M. Couton, S. K. Warfield and K. Miller (2010). "Patient-specific non-linear finite element modelling for predicting soft organ deformation in real-time; Application to non-rigid neuroimage registration." Progress in Biophysics and Molecular Biology **103**: 292-303.